Arrhythmia Classification Based on Adaptive Refined Composite Multiscale Fluctuation Dispersion Entropy

Changsheng Zhang, Xin Ding[*], Changping Tian, Wei Peng

The Faculty of Information Engineering and Automation
Kunming University of Science and Technology
Kunming 650500, China
E-mails: 18726111568@163.com, Shixin_Ding@outlook.com,
1759256468@qq.com, 749049662@qq.com

[*]*Corresponding author*

Abstract: To improve the accuracy of electrocardiography (ECG) signal classification and identify abnormal heart rhythms, an arrhythmia classification algorithm based on adaptive refined composite multiscale fluctuation dispersion entropy (ARCMFDE) is proposed. First, an improved QRS complex detection algorithm named the improved Pan-Tompkins algorithm (IPTA) is used. The QRS wave is detected, and the waveform is further processed; then, the signal is decomposed into multiple modal components using variational mode decomposition with the optimized number of decomposition layers (K). Subsequently, the RCMFDE is extracted from the different modal components as a classification feature. Finally, differential evolution (DE) and grey wolf optimization (GWO) are combined to form the hybrid differential evolution-grey wolf pack optimization (DE-GWO) algorithm to optimize the penalty factor c and the kernel function parameter g of the support vector machine for performing pattern recognition. Experimental results show that compared with other methods such as variational mode decomposition (VMD), fluctuation dispersion entropy (FDE), genetic algorithms (GA), and support vector machine (SVM). The proposed classification model has superior performance, with an average accuracy of 96.1%, a sensitivity of 95.9%, and a specificity of 98.7% for four types of heart rhythm recognition. Thus, accurate classification of ECG signals can be achieved using the proposed ARCMFDE-based DE-GWO method.

Keywords: Arrhythmia classification, Variational mode decomposition, Adaptive refined composite multiscale fluctuation dispersion entropy, Differential evolution – Grey wolf optimization – Support vector machines.

Introduction

Arrhythmias usually include conditions such as atrial fibrillation, ventricular fibrillation, and tachycardia. Unlike a single arrhythmia, continuous arrhythmias can affect the lives and health of people. Understanding the health of the heart and saving patients' lives requires an accurate and prompt diagnosis of aberrant cardiac rhythms. Because electrocardiography (ECG) signals are nonstationary, ideal results cannot be achieved by using classification methods based on a single feature; therefore, fusion algorithms have gained popularity in ECG signal classification research.

Empirical mode decomposition (EMD) is suitable for the time-frequency analysis of nonlinear and nonstationary signals; however, the modal mixing phenomena affect this process [7, 8]. In 2014, Dragomiretskiy and Zosso [6] proposed the variational mode decomposition (VMD) method as a nonrecursive adaptive signal decomposition approach with high computational accuracy and operational efficiency, effectively using multiple adaptive Wiener filters. It has

good robustness and may overcome the shortcomings of EMD [1, 3, 6, 17]. The entropy value shows the degree of chaos in the time series, and three methods based on information entropy are typically employed for feature extraction: (1) Permutation entropy has a high calculation speed and can effectively measure the complexity of the signal; however, it does not consider the difference between the average amplitude and the amplitude of the waveform [13]; (2) Sample entropy exhibits low computation speed and poor real-time performance and its similarity metric is prone to sudden changes [10]; (3) Fuzzy entropy is used to measure the probability of generating a new pattern as the dimensionality changes; the higher the probability, the higher the fuzzy entropy [15]. In 2016, Rostaghi and Azami [16] proposed dispersion entropy, which overcomes disadvantages such as the slow computation of permutation entropy for large-scale data, is less affected by mutant signals and considers the height difference between amplitudes. Fluctuation dispersion entropy (FDE) proposed by Azami and Escudero [4] in 2018 is more stable and has a well-detrended performance. The methods discussed above are single-scale analysis methods based on time series, and their entropy values do not fully incorporate arrhythmia information. Azami et al. [5] proposed refined composite multiscale fluctuation dispersion entropy (RCMFDE) based on FDE. RCMFDE is obtained by multiscale quantization of the signal based on dispersion entropy, which deals with nonlinear and nonstationary biological signals more effectively.

The essence of arrhythmia classification lies in pattern recognition. Acharya et al. [2] proposed an 11-layer deep convolutional neural network model to automatically classify four types of rhythm signals in the MIT-BIH arrhythmia database. The accuracy, sensitivity, and specificity in the classification of 2 s ECG segments reached 92.50%, 98.09%, and 93.13% and those in the classification of 5 s ECG segments reached 94.90%, 99.13%, and 81.44% [2], respectively. Based on the object-oriented classification approach, Li and Zhou [11] proposed to apply wavelet packet entropy and random forest to ECG classification and used the entropy value of ECG signal wavelet decomposition as the feature to build a random forest classification model. The model achieved 94.61% accuracy. Kachuee et al. [9] used a deep convolutional neural network to classify ECG signals; however, the neural network requires a long computation time and is difficult to scale up [11]. Because of its advantages in handling nonlinear problems with a small sample size, support vector machines (SVMs) are commonly used. In this study, the grey wolf optimization (GWO) algorithm [14], a new metaheuristic optimization algorithm with a high convergence speed and strong global optimality search capability, is introduced to search for the optimality of the SVM for the easy selection of relevant parameters of the SVM. However, the GWO algorithm has trouble effectively preserving population variety, resulting in a local optimum. As a result, a differential evolution (DE) method [18] is added to the GWO algorithm in this study, resulting in a more efficient hybrid differential evolution-grey wolf optimization algorithm (hereinafter, DE-GWO) with improved global search capabilities.

In summary, the study proposes an ARCMFDE-based arrhythmia classification method. First, the ECG signal is decomposed into multi-modal components by VMD with the optimized number of decomposition layers (K), and the RCMFDE is extracted as the feature vector for different modal components. Second, the parameters of the SVM are optimized by the DE-GWO. Finally, the identification performance of classification methods using dispersion entropy and fluctuation dispersion entropy is compared. The results validated the proposed method's superiority.

Data preprocessing
In this study, to filter out the noise in the ECG signal and reduce the effects of other waveforms such as P-wave and T-wave on the QRS complex waveform, the improved Pan-Tompkins

algorithm (IPTA) is used to detect and identify the QRS wave [18]. As shown in Figs. 1a to 1e, record No. 103 of the MIT-BIH arrhythmia database is first processed by the finite impulse response (FIR) bandpass filter with a passband frequency of 15-25 Hz and then further processed by the double-slope method. Subsequently, the FIR low-pass filter (parameters: window function, 19th order, cut-off frequency = 5 Hz, sampling frequency = 360 Hz) is used to filter out high-frequency signals and eliminate the bimodal phenomenon.

a) original signal

b) bandpass filtering

c) "double slope" processing

d) low-pass filtering

e) sliding window credits

f) adaptive threshold

f) localization of QRS waves
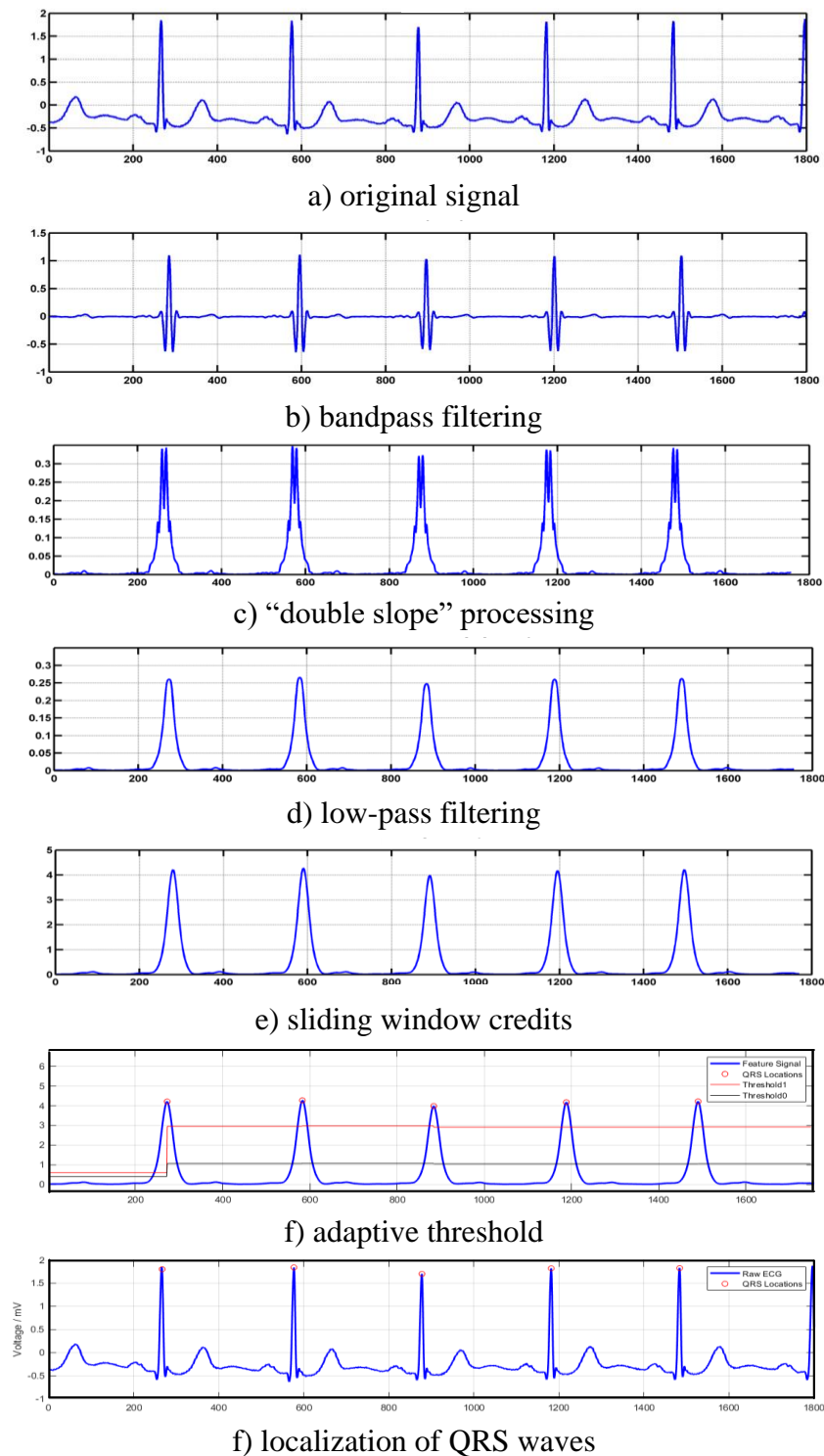
Fig. 1 Detection of the QRS complex

However, this process will further reduce the signal amplitude, making it unfavourable for detection. As a result, a sliding window integral is utilized to boost the waveform's absolute amplitude. After that, adaptive thresholds are used to detect the QRS waveform, and the high and low thresholds (T_1 and T_0) can be modified in real-time when the waveform amplitude varies, as shown in Eq. (1) and Eq. (2) below:

$$T_1 = \begin{cases} 0.7 * mean(peak\_v8), \text{ if } (peak > T_1) \\ T_1 - \dfrac{\left| peak - mean(peak\_v8) \right|}{2}, \text{ if } (T_0 < peak < T_1) \\ T_{1\_}lim, \text{ if } (T_1 \leq T_{1\_}lim) \end{cases} \tag{1}$$

$$T_0 = \begin{cases} 0.25 * mean(peak\_v8), \text{ if } (peak > T_1) \\ 0.4 * peak, \text{ if } (T_0 < peak < T_1) \\ T_{0\_}lim, \text{ if } (T_0 \leq T_{0\_}lim) \end{cases} \tag{2}$$

where the *peak* is the detected peak, $peak\_v8$ indicates the storage location of the first eight detected peaks of the current detected wave, $T_{1\_}lim$ and $T_{0\_}lim$ are the lower limits of two thresholds (taken as 0.3 and 0.23), and *mean*(.) is the mean value of the content in parentheses. The detection findings of QRS waveforms are presented in Figs. 1f and 1g using record No. 119 as an example (Fig. 1g).

A whole heartbeat is made up of waveforms like the P-wave, T-wave, and QRS wave, and it lasts about 0.7 s. The heartbeat interception is usually achieved by considering several sampling points considered forward and backward from the position of the R-peak, and then this section of sampling points is intercepted as a heartbeat. In this study, 100 points to the left and 150 points to the right were taken, implying that the length of each heartbeat is 250 samples (with a sampling frequency of 360 Hz for approximately 0.7 s). Finally, the left bundle branch block (L), right bundle branch block (R), premature ventricular beats (V), and normal condition heartbeat waveforms were obtained (N). Fig. 2 depicts the waveforms.

Feature extraction
Variational mode decomposition
VMD first requires a constrained variational model [20]:

$$\begin{cases} \min\limits_{\{u_k\},\{\omega_k\}} \left\{ \sum\limits_{k=1}^{K} \left\| \partial_t \left[\left(\delta(t) + \dfrac{j}{\pi t} \right) u_k(t) \right] e^{-j\omega_k t} \right\|_2^2 \right\}, \\ \text{s.t. } \sum\limits_{k=1}^{K} u_k = f(t) \end{cases} \tag{3}$$

where $f(t)$ is the original signal, $u_k(t)$ is the kth intrinsic mode function (IMF) component, and ω_k is the centre frequency of the kth IMF component.

a) left bundle branch block   b) right branch block

c) normal   d) ventricular premature beats
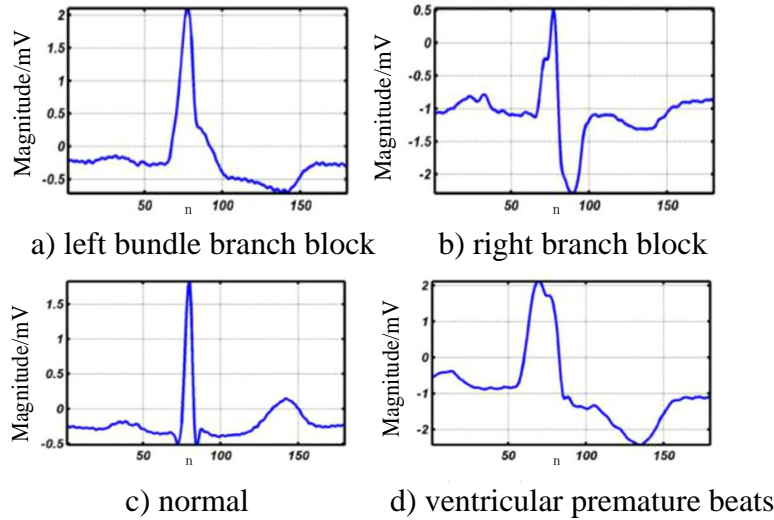
Fig. 2 Waveforms of typical heartbeats

By introducing the penalty factor α and the Lagrange multiplier operator $\lambda(t)$ in the modal, the constrained variational problem is converted into an unconstrained variational problem. Then, the extended Lagrangian function is obtained, and u^{n+1}, ω^{n+1}, and λ^{n+1} are iteratively updated with the alternating method of the multiplier operator. The above steps are repeated until the following equation is satisfied to obtain k^{th} IMF components.

$$L\left(\{u_k\},\{\omega_k\},\lambda\right)=\alpha\sum_k\left\|\partial_t\left[\left(\delta(t)+\frac{j}{\pi t}\right)u_k(t)\right]e^{-j\omega_k t}\right\|_2^2+$$
$$+\left\|f(t)-\sum_k u_k(t)\right\|_2^2+\langle\lambda(t),\ f(t)-\sum_k u_k(t)\rangle \tag{4}$$

$$\sum_k\left(\left\|\hat{u}_k^{n+1}-\hat{u}_k^n\right\|_2^2/\left\|\hat{u}_k^n\right\|_2^2\right)<\varepsilon. \tag{5}$$

The following approach for determining the K value can be utilized in the process of adaptive decomposition using VMD to avoid the phenomena of under or over-decomposition [19].

The input signal is processed by VMD using the minimal modal number $K = 3$ and the following equation is used to determine whether over-decomposition occurs.

$$\min\left(\left\|\frac{\omega_{i+1}-\omega_i}{(\omega_{i+1}+\omega_i)/2}\right\|\right)\leq\mu. \tag{6}$$

Set $K = K - 1$ and end the loop if Eq. (6) is met. Otherwise, set $K = K + 1$ and repeat the preceding steps.

Refined composite multiscale fluctuation dispersion entropy

A time series of length N, $x = \left\{ x_j, \ j = 1, 2, ..., N \right\}$, is mapped to $y = \left\{ y_j, \ j = 1, 2, ..., N \right\}$ using the function as follows:

$$y_j = \frac{1}{\sqrt{2\pi}\sigma} \int_{-\infty}^{x_j} e^{-\frac{(t-\mu)^2}{2\sigma^2}} \, dt, \ y_j \in (0, 1), \tag{7}$$

where μ and σ are the time series' mean and standard deviation, respectively.

Using linear transformations to map y to the range of [1, 2, ..., c], we obtain:

$$z_j^{(c)} = \text{int}\left(cy_j + 0.5 \right), \tag{8}$$

where c is the number of categories, int denotes rounding and $z_j^{(c)}$ denotes the categorized time series' j^{th} element.

Eq. (9) is used to calculate the embedding vector:

$$z_j^{(m, c)} = \left(z_i^{(c)}, \ z_{i+d}^{(c)}, \ ..., \ z_{i+(m-1)d}^{(c)} \right), \ i = 1, 2, ..., N - (m-1)d, \tag{9}$$

where m and d are the embedding dimension and time delay, respectively.

If $z_i^{(c)} = v_0$, $z_{i+d}^{(c)} = v_1$, ..., $z_{i+(m-1)d}^{(c)} = v_{m-1}$, then the dispersion pattern of $z_j^{(m, c)}$ is $\pi_{v_0 v_1 ... v_{m-1}}$, and the probability of each dispersion mode is:

$$p\left(\pi_{v_0 v_1 ... v_{m-1}} \right) = \frac{num\left(\pi_{v_0 v_1 ... v_{m-1}} \right)}{N - (m-1)d}, \tag{10}$$

where $num\left(\pi_{v_0 v_1 ... v_{m-1}} \right)$ is the number of maps from $z_j^{(m, c)}$ to $\pi_{v_0 v_1 ... v_{m-1}}$.

The RCMFDE value is defined as the average of the coarse-grained sequence's dispersion entropy, and τ corresponds to the multiple starting points of the coarse-grained process. The kth coarse-grained sequence of the signal x is listed as follows:

$$x_k^{(\tau)} = \left\{ x_{k,1}^{(\tau)}, \ x_{k,2}^{(\tau)}, \ ... \right\}, \tag{11}$$

$$x_{k,j}^{(\tau)} = \frac{1}{\tau} \sum_{b=k+\tau(j-1)}^{k+\tau j-1} u_b, \ 1 \le j \le N, \ 1 \le k \le \tau. \tag{12}$$

RCMFDE at scale τ is defined as follows:

$$RCMFDE\left(x, m, c, d, \tau\right) = -\sum_{\pi=1}^{(2c-1)^{m-1}} In\left(\bar{p}\left(\pi_{v_0v_1...v_{m-1}}\right)\right)\bar{p}\left(\pi_{v_0v_1...v_{m-1}}\right) \tag{13}$$

where $\bar{p}\left(\pi_{v_0v_1...v_{m-1}}\right)$ is the average of the probabilities of the dispersion patterns corresponding to the coarse-grained sequences, $p_k^{(\tau)}$ is the probability of dispersion patterns corresponding to the kth coarse-grained sequences at scale τ.

Adaptive refined composite multiscale fluctuation dispersion entropy

To overcome the shortcomings of RCMFDE features, the information entropy features are improved. Based on the increased information entropy characteristics, an ARCMFDE feature extraction approach is proposed. First, the ECG signal is adaptively decomposed using VMD to obtain a preset number of IMF components; then RCMFDE is extracted from the decomposed different variational modal functions as features. The pseudo-code for the method is described below, and the flow chart is displayed in Fig. 3.

1. begin
2. **for** $i = 1:q$, $L = 1:K$
4.   Perform VMD decomposition
5.   **while** $K \geq 3$
6.   **do**
7.   **if** $\left(\min\left(\left|\dfrac{\omega_{i+1} - \omega_i}{(\omega_{i+1} + \omega_i)/2}\right|\right) > \mu\right)$
8. $K = K + 1;$
9.   **if** $\left(\min\left(\left|\dfrac{\omega_{i+1} - \omega_i}{(\omega_{i+1} + \omega_i)/2}\right|\right) \leq \mu\right)$
10. $K = K - 1;$
11.   **end if**
12. **end for**
13. **do**
14.   According to
        $$RCMFDE\left(x, m, c, d, \tau\right) =$$
        $$-\sum_{\pi=1}^{(2c-1)^{m-1}} In\left(\bar{p}\left(\pi_{v_0v_1...v_m}\right)\right)\bar{p}\left(\pi_{v_0v_1...v_{m-1}}\right)$$
15.   Calculate RCMFDE features
16.   **end do**
17. **end begin**
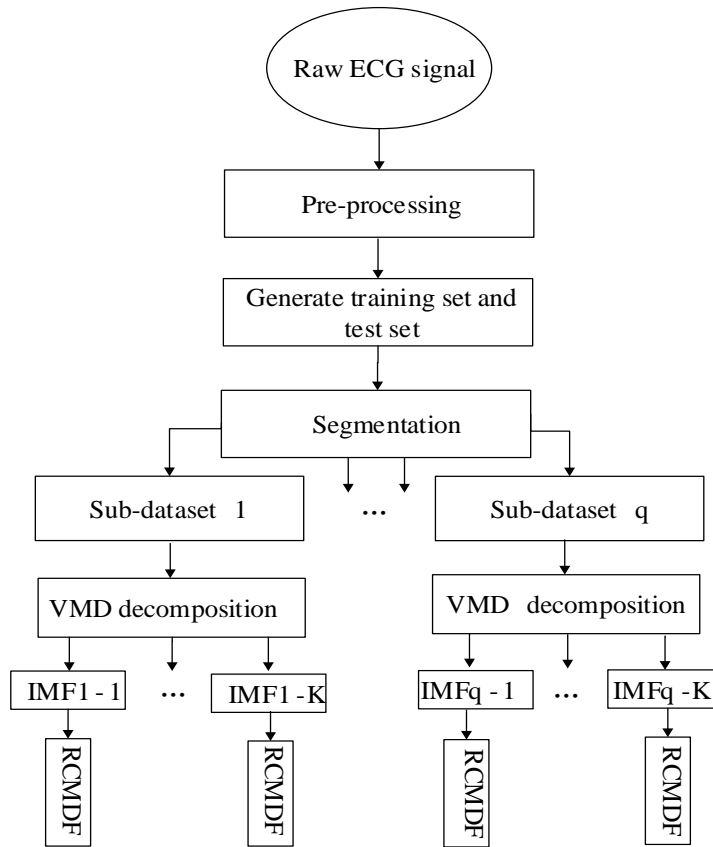
Fig. 3 ARCMFDE feature extraction process

Differential grey wolf hybrid optimization algorithm

Wolves usually hunt in a packing envelope, modelled as follows:

$$\begin{cases} D = \left| C X_p(t) - X(t) \right| \\ X(t+1) = X_p(t) - AD \\ A = 2ar_1 - a \\ C = 2r_2 \end{cases}, \tag{14}$$

where t is the number of iterations, A and C are vector coefficients, X_p is the orientation of the prey, and X is the wolf pack orientation. Drops linearly from 2 to 0, while r_1 and r_2 are random values in the range [0, 1] [19]. Wolf packs detect the presence of prey and take the lead in a siege. The optimal solution is defined as the location of the alpha wolf. The individual wolf moves in the direction of the prey based on the distance between itself and the alpha wolf in the first three levels; this is stated in Eq. (15):

$$\begin{cases} D_a = \left| C_1 X_\beta - X \right|, \ D_\beta = \left| C_2 X_\beta - X \right| \\ D_\delta = \left| C_3 X_\delta - X \right|, \ X_1 = X_a - A_1 D_a \\ X_2 = X_\beta - A_2 D_\beta, \ X_3 = X_\delta - A_3 D_\delta \\ X(t+1) = (X_1 + X_2 + X_3) / 3 \end{cases} \tag{15}$$

The DE algorithm is capable of doing a quick and efficient merit search [18]. The vector difference of two randomly selected individuals in the initial population is scaled and added to an unmutated individual in the population during mutation. The exchange of some elements between the new person created by mutation and the unmutated individual is known as crossover. Selection occurs when the new individual created by mutation and crossover outperforms the parent. In all other cases, the parent is kept.

The DE algorithm's crossover and mutation operations are first utilized to maintain population variety; the mutated grey wolf operator is then formed and added to the GWO algorithm's starting population to create a mixed initial population of grey wolves and mutant grey wolves. The objective function values of the individuals are then calculated to choose the best three: X_α, X_β, and X_δ. Finally, the positions of other grey wolves are updated to reflect the new information. The DE algorithm is used to cross the wolves to new hybrid individuals and to change their locations to α, β, and δ wolves. The selection operation iteratively updates the placements of the wolf individuals until the ideal objective function value is picked for output. The hybrid algorithm can improve global search ability and solve the single-feature algorithm's difficulties of premature stagnation, poor stability, sliding into local optimum, and low search efficiency, combining the two algorithms' complementing advantages.

The suggested optimization algorithm's performance is verified through a test analysis utilizing the standard functions presented in Table 1 and a comparison of the DE-GWO algorithm to other optimization algorithms.

Table 1. Standard testing functions

Function name	Function expressions	Dimension	Range of values	Optimum value
Sphere	$f_1(x) = \sum_{i=1}^{d} x_i^2$	30	$[-100, 100]$	0
Ackley	$f_2(x) = -20\exp\left(-0.2\sqrt{\frac{1}{n}\sum_{i=1}^{d} x_i^2}\right) - \exp\left(-\frac{1}{n}\sqrt{\sum_{i=1}^{d}\cos(2\pi x_i)}\right) + 20 + e$	30	$[-32, 32]$	0
Rastrigin	$f_3(x) = \sum_{i=1}^{d}\left(x_i^2 - 10\cos(2\pi x_2) + 10\right)$	30	$[-5.12, 5.12]$	0
Rosenbrock	$f_4(x) = \sum_{i=1}^{d-1}\left(100(x_{i+1} - x_i^2) + (x_{i+1} - 1)^2\right)$	30	$[-30, 30]$	0
Griewank	$f_5(x) = \frac{1}{4000}\left(\sum_{i=1}^{n} x_i^2\right) - \left(\prod_{i=1}^{n}\cos\left(\frac{x_i}{\sqrt{i}}\right)\right) + 1$	30	$[-600, 600]$	0

The parameters of DE-GWO and GWO algorithms were set as follows:
- wolf pack size = 30;
- maximum scaling factor = 1.5;
- minimum scaling factors = 0.25;
- crossover probability = 0.7;
- maximum number of iterations = 500;

- elimination update scale factor = 0.618.

The particle swarm optimization (PSO) method settings were set as follows:
- number of particles = 30;
- learning factor = 2;
- inertia weight = 0.9.

The algorithm's optimization performance was assessed using the standard test functions mentioned in Table 1, with the results presented in Table 2.

Table 2. Test results of different optimization algorithms

Algorithms	Result values	f_1	f_2	f_3	f_4	f_5
PSO	optimal	3.134	2.006	25.769	23.128	0.876
PSO	mean	89.412	5.842	39.936	46.101	5.427
GWO	optimal	2.122×10^{-25}	6.438×10^{-12}	8.096	5.652	0
GWO	mean	1.679×10^{-22}	1.002×10^{-11}	14.027	9.021	0.043
DE-GWO	optimal	4.002×10^{-50}	1.601×10^{-15}	3.396×10^{-9}	3.294×10^{-4}	0
DE-GWO	mean	1.803×10^{-46}	1.197×10^{-14}	2.286×10^{-8}	0.168	3.497×10^{-10}

These results indicate that the DE-GWO optimization algorithm outperforms other conventional algorithms.

Analysis of experiments and results

The arrhythmia classification process is presented in Fig. 4.
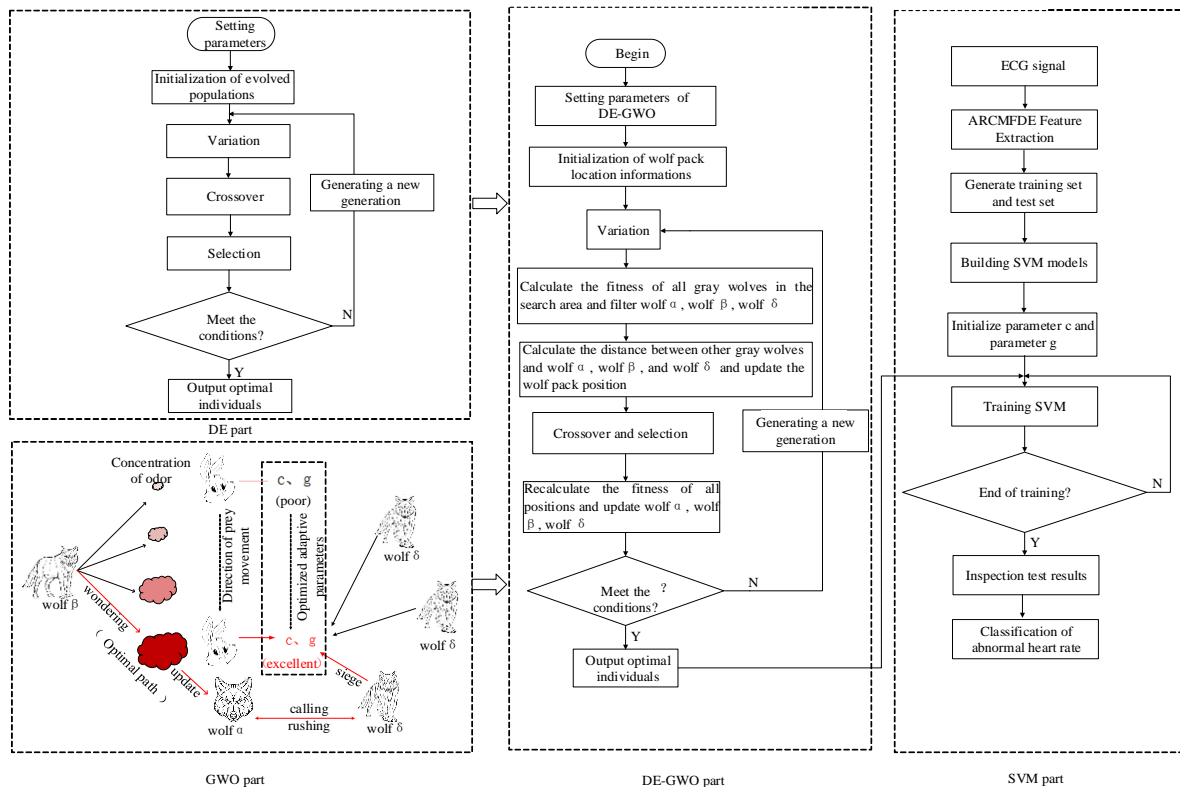
Fig. 4 Arrhythmia classification process

The data for this study were obtained from the MIT-BIH arrhythmia database, which contains 48 ECG records with a sampling frequency of 360 Hz. The 48 ECG records were processed and the heartbeat signals were segmented to check the effect of categorization; a total of 97 318 heartbeat signals in four categories were eventually retrieved. As shown in Table 3, among the four types of heartbeats, the number of normal (N) heartbeats was 74 962, the number of premature ventricular (V) heartbeats was 7 034, the number of right bundle branch block (R) heartbeats was 7 254, and the number of left bundle branch block (L) heartbeats was 8 068. Considering the balance of the sample, in this study, 2 000 heartbeats were selected for each category, a total 8 000 samples.

Table 3. Number of various heartbeats

Types of heartbeats	Number of heartbeats
N	74 962
V	7 034
R	7 254
L	8 068
Total	97 318

ARCMFDE feature extraction

The ECG sequence can be decomposed into K IMF components by using VMD; each component is rich in ECG information. The K value set empirically has a large influence on the decomposition effect, and in this study, the optimal K value is selected by the distribution of central frequencies. Table 4 shows the centre frequencies corresponding to each IMF component at different K values for record No. 103.

Table 4. The corresponding centre frequency
of each intrinsic modal component at different K values

K value	Centre frequency, Hz					
	IMF1	**IMF2**	**IMF3**	**IMF4**	**IMF5**	**IMF6**
3	1.43×10^{-4}	0.0263	0.4920			
4	1.42×10^{-4}	0.0262	0.4593	0.4931		
5	7.37×10^{-5}	0.0176	0.0392	0.4700	0.4934	
6	7.28×10^{-5}	0.0173	0.0371	0.4480	0.4815	0.4955

Table 4 shows that when the number of decomposition layers K is 3, the centre frequencies of the IMF components differ greatly, making it difficult to achieve effective decomposition of the signal; this phenomenon is called under-decomposition. When the number of decomposition layers K is 5 and 6, the centre frequencies of some IMF components are relatively close to each other, leading to modal mixing; this phenomenon is over-decomposition. To prevent over- or under-decomposition, the optimal number of decomposition layers is determined as 4. Fig. 5 shows the four types of heartbeats decomposed by four VMD layers.

a) left bundle branch block

b) right bundle branch block

c) ventricular premature beats

d) normal
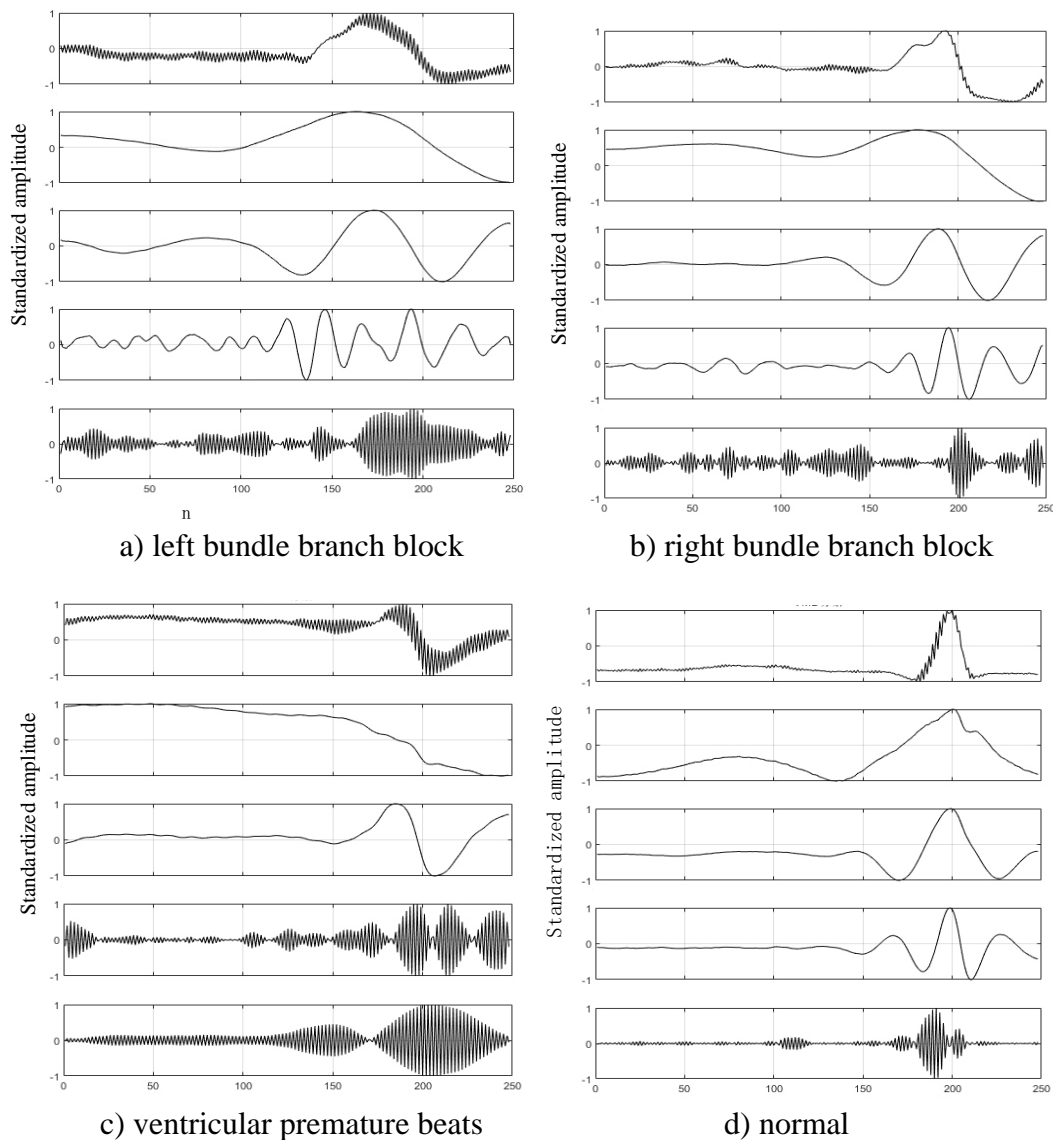
Fig. 5 Types of heartbeats subjected to four layers of decomposition

Fig. 5 shows that the four types of original heartbeat waveform show different degrees of burrs due to the effect of noise. VMD results in a fourth-order times series component from low to high frequencies, with each IMF component being relatively independent and without large modal mixing. The high-order components show a certain fusiform envelope. The instantaneous frequencies of the generated analytic signals have real physical meaning, thanks to VMD's effective separation of the modal components. According to Eq. (13), four parameters are required to calculate RCMFDE, namely embedding dimension m, the number of categories c, time delay d, and scale factor τ. In this study, m was considered as 2 or 3, c was an integer ranging from 4-8, d was taken as 1, and τ, which determines the coarse granularity of the signal, was taken as 3. To choose a suitable τ value, the maximum value of τ was first set to 15. Subsequently, the four rhythm signals, namely left bundle branch block, right bundle branch block, premature ventricular beats, and normal beats, were processed by VMD combined with the proposed RCMFDE algorithm to obtain the multiscale features of multiple modal components. Finally, the results are plotted as line plots as shown in Fig. 6.
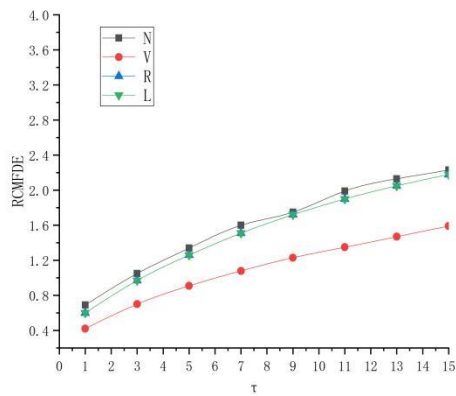
a) mean value of *RCMFDE*
of the first-order modal component
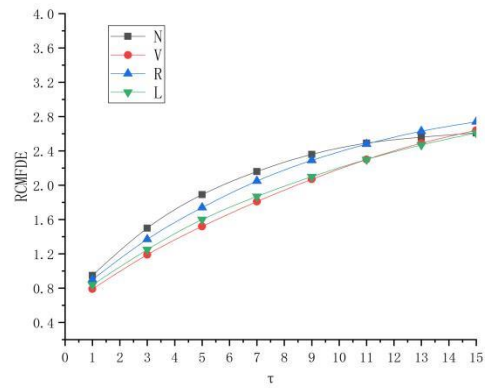
b) mean value of *RCMFDE*
of the second-order modal component
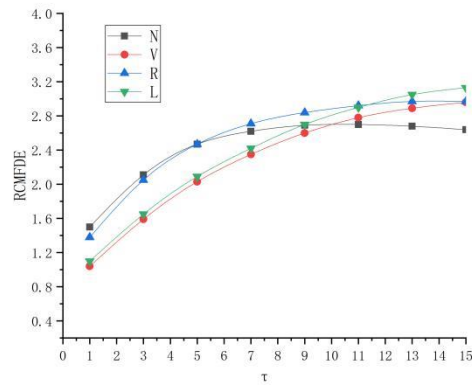
c) mean value of *RCMFDE*
of the third-order modal component
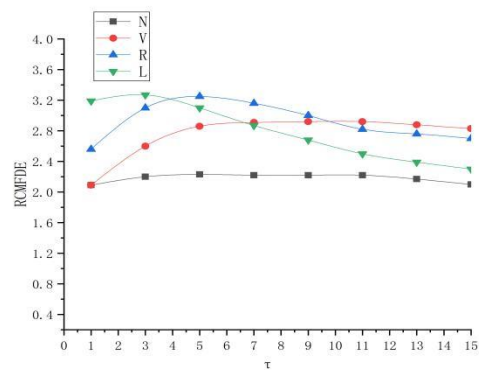
d) mean value of *RCMFDE*
of the fourth-order modal component

Fig. 6. Mean RCMFDE of heart rhythm signals

Fig. 6 indicates that for the same rhythm, different modal components have different RCMFDE values at various scales. With increasing scale factor, the mean RCMFDE value climbs at first, then drops; further, it tends to be stable beyond a scale factor τ of 10. Although there is an increase or even a crossover at individual scales, the overall decreasing trend of the RCMFDE value is not affected.

DE-GWO-SVM classification recognition

To verify the effectiveness of the proposed method, the extracted ARCMFDE features were input to a DE-GWO-optimized SVM classifier for pattern recognition. The penalty factor c and the kernel function parameter g were searched for optimality by DE-GWO. The relevant parameters of DE-GWO were set as follows:

- number of iterations = 200;
- population size = 30;
- crossover probability = 0.4;
- scaling factor W ranged from 0.3 to 1.5;
- penalty factor c ranged from 0 to 100;
- kernel function parameter g ranged from 0 to 1000.

The optimal parameters *c* and *g* after DE-GWO optimization were 1.94 and 23.76, respectively. The DE-GWO-SVM evolution curve is shown in Fig. 7.
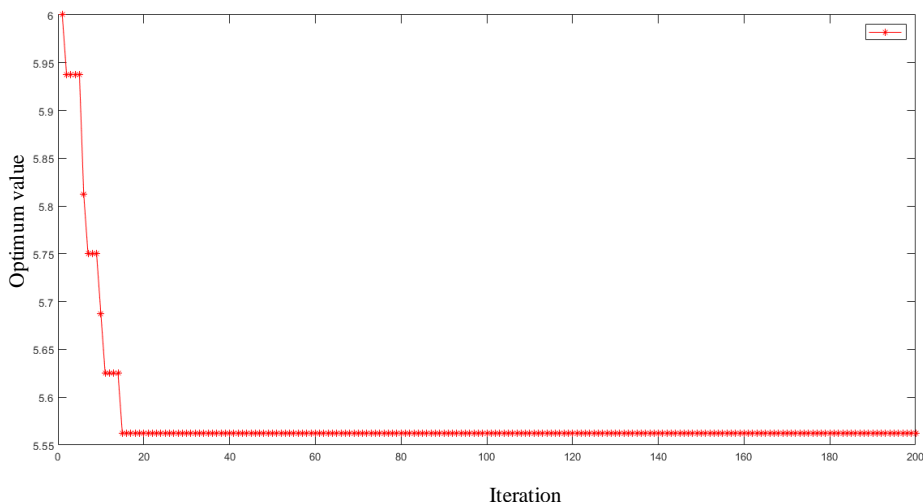

Fig. 7 DE-GWO-SVM evolution curve

The accuracy (Acc), sensitivity (Se), and specificity (Sp) of the classification findings were evaluated. The classification accuracy of DE-GWO-SVM for the four types of heartbeats was 97.3% (N), 92.8% (V), 96.5% (R), and 97.8% (L), with an average classification accuracy of 96.1%. Fig. 8 depicts the classification findings using a confusion matrix representation model, in which 11 N-, 29 V-, 14 R-, and 9 L-type heartbeats are misdiagnosed as other heartbeats. Table 5 examines the categorization accuracy, sensitivity, and specificity of the four types of heartbeats.

Fig. 8 Classification results of the GA-SVM classifier

Furthermore, the dispersion entropy and fluctuation dispersion entropy features of the signal were extracted and fed to Bayesian, decision tree, *K*-nearest neighbour (KNN), SVM, GA-SVM, and DE-GWO-SVM classifiers for pattern recognition. The accuracy of several classification algorithms is compared in Table 6.

Table 5. Indicators of the four heartbeat classification results

Indicators	DE-GWO-SVM			
	N	V	R	L
Ac	97.3%	92.8%	96.5%	97.8%
Se	95.6%	98.1%	91.0%	98.7%
Sp	99.1%	97.6%	98.8%	99.2%

Table 6. Comparison of accuracy of different classification methods

Features	Methods of classification					
	Bayes	Decision tree	KNN	SVM	GA-SVM	DE-GWO-SVM
VMD-DE	89.2%	90.0%	91.5%	93.2%	94.1%	95.4%
VMD-FDE	90.4%	92.3%	92.5%	94.4%	95.3%	95.9%
ARCMFDE	92.0%	93.5%	93.8%	94.7%	95.8%	96.1%

As shown in Table 6, when ARCMFDE is used as the feature, the recognition accuracy is 92.0%, 93.5%, 93.8%, 94.7%, 95.8%, and 96.1% with Bayes, decision tree, KNN, SVM, GA-SVM, and DE-GWO-SVM classifiers, respectively. Moreover, the recognition accuracy with DE-GWO-SVM is 95.4%, 95.9%, and 96.1% using VMD-DE, VMD-FDE, and ARCMFDE as the feature, respectively. The findings show that the proposed ARCMFDE-based DE-GWO-SVM algorithm has a greater recognition accuracy than existing techniques.

Conclusion

An ARCMFDE-based arrhythmia classification method was proposed in this paper. First, the *K* value of VMD decomposition was optimized to avoid over- and under-decomposition. Then, the RCMFDE features were extracted from multiple IMFs after VMD. Finally, the SVM's penalty factor c and kernel function parameter g were searched and optimized for classification recognition by the DE-GWO algorithm. By using the samples from the MIT-BIH arrhythmia database, the proposed method could achieve an average identification accuracy of 96.1%, a sensitivity of 95.6%, and a specificity of 98.7% for four types of heart rhythms. Compared with algorithms such as the VMD-FDE-based GA-SVM, the proposed method could maximize the extraction of effective features of ECG signals and achieve accurate classification of arrhythmias. As a result, an excellent approach for diagnosing arrhythmias has been presented.

Acknowledgements

Ethical approval
All procedures performed in studies involving human participants were by the ethical standards of the institutional and/or national research committee and with the 1964 Helsinki Declaration and its later amendments or comparable ethical standards.

References

1. Abdoos A., P. K. Mianaei, M. R. Ghadikolaei (2016). Combined VMD-SVM Based Feature Selection Method for Classification of Power Quality Events, Applied Soft Computing, 38(3), 637-646.
2. Acharya U. R., H. Fujita, S. L. Oh, Y. Hagiwara, J. H. Tan, M. Adam (2017). Application of Deep Convolutional Neural Network for Automated Detection of Myocardial Infarction Using ECG Signals, Information Sciences, 415, 190-198.
3. Aneesh C., S. Kumar, P. M. Hisham, K. P. Soman (2015). Performance Comparison of Variational Mode Decomposition over Empirical Wavelet Transform for the Classification of Power Quality Disturbances using Support Vector Machine, Procedia Computer Science, 46, 372-380.
4. Azami H., J. Escudero (2018). Amplitude- and Fluctuation-based Dispersion Entropy, Entropy, 20(3), 210.
5. Azami H., S. E. Arnold, S. Sanei, Z. Chang, G. Sapiro, et al. (2019). Multiscale Fluctuation-based Dispersion Entropy and Its Applications to Neurological Diseases, IEEE Access, 7, 68718-68733.
6. Dragomiretskiy K., D. Zosso (2014). Variational Mode Decomposition, IEEE Transactions on Signal Processing, 62(3), 531-544.
7. Huang N. E., Z. H. Wu (2009). Ensemble Empirical Mode Decomposition: A Noise-assisted Data Analysis Method, Advances in Adaptive Data Analysis, 1(1), 1-41.
8. Huang N. E., Z. Shen, S. R. Long, M. C. Wu, H. H. Shih, et al. (1998). The Empirical Mode Decomposition and the Hilbert Spectrum for Nonlinear and Non-stationary Time Series Analysis, Proceedings of the Royal Society of London. Series A: Mathematical, Physical and Engineering Sciences, 454(1971), 903-995.
9. Kachuee M., S. Fazeli, M. Sarrafzadeh (2018). ECG Heartbeat Classification: A Deep Transferable Representation, 2018 IEEE International Conference on Healthcare Informatics (ICHI), 443-444.
10. Lake D. E., J. S. Richman, M. P. Griffin, J. R. Moorman (2002). Sample Entropy Analysis of Neonatal Heart Rate Variability, American Journal of Physiology-regulatory, Integrative and Comparative Physiology, 283(3), R789.
11. Li T., M. Zhou (2016). ECG Classification Using Wavelet Packet Entropy and Random Forests, Entropy, 18(8), 285.
12. Li W. (2020). ECG Signal Recognition and Classification Based on Feature Extraction and Neural Network Integration, PhD Thesis, Qilu University of Technology, 25-40.
13. Li Y. X., Y. A. Li, Z. Chen, X. Chen (2016). Feature Extraction of Ship-radiated Noise Based on Permutation Entropy of the Intrinsic Mode Function with the Highest Energy, Entropy, 18(11), 393.
14. Mirjalili S., S. M. Mirjalili, A. Lewis (2014). Grey Wolf Optimizer, Advances in Engineering Software, 69, 46-61.
15. Morente-Molinera J. A., J. Mezei, C. Carlsson, E. Herrera-Viedma (2016). Improving Supervised Learning Classification Methods Using Multigranular Linguistic Modeling and Fuzzy Entropy, IEEE Transactions on Fuzzy Systems, 25(5), 1078-1089.
16. Rostaghi M., H. Azami (2016). Dispersion Entropy: A Measure for Time-series Analysis, IEEE Signal Processing Letters, 23(5), 610-614.
17. Salim L. (2014). Comparative Study of Signal Denoising by Wavelet Threshold in Empirical and Variational Mode Decomposition Domains, Healthcare Technology Letters, 1(3), 104-109.
18. Storn R., K. Price (1997). Differential Evolution – A Simple and Efficient Heuristic for Global Optimization over Continuous Spaces, Journal of Global Optimization, 11(4), 341.

19. Wang H., Q. Wang, F. Hu (2019). Are You Afraid of Heights and Suitable for Working at Height?, Biomedical Signal Processing and Control, 52, 23-31.
20. Yang H., K. Zhao, G. Li (2019). A New Ship-radiated Noise Feature Extraction Technique Based on Variational Mode Decomposition and Fluctuation-based Dispersion Entropy, Entropy, 21(3), 235.

Changsheng Zhang, M.Sc.
E-mail: 18726111568@163.com

Changsheng Zhang obtained his M.Sc. Degree from Kunming University of Science and Technology in the period 1998-2001. He has worked in the Faculty of Information Engineering and Automation of Kunming University of Science and Technology, Kunming, China, since 2002. His field of interest covers medical signal processing, swarm intelligence optimization algorithms, complex industrial modelling, and image processing.

Xin Ding, M.Sc. Student
E-mail: Shixin_Ding@outlook.com

Xin Ding obtained her B.Sc. Degree from Kunming University of Science and Technology in the period 2017-2021. Currently, she is studying in the Faculty of Information Engineering and Automation at Kunming University of Science and Technology, Kunming, China. Her field of interest covers medical signal processing, swarm intelligence optimization algorithms, and complex industrial modelling.

Changping Tian, M.Sc.
E-mail: 1759256468@qq.com

Changping Tian obtained his M.Sc. Degree from Kunming University of Science and Technology in the period 2019-2022. Currently, he is working in Henan Province, China. His field of interest covers medical signal processing, bioinformatics, and medical imaging.

Wei Peng, Ph.D.
E-mail: 749049662@qq.com

Wei Peng obtained her Ph.D. Degree from Central South University in the period 2010-2013. She has worked in the Faculty of Information Engineering and Automation of Kunming University of Science and Technology, Kunming, China, since 2014. Her field of interest covers machine learning, data mining, bioinformatics, and medical imaging.